Acta Oceanol. Sin., 2019, Vol. 38, No. 4, P. 39–46
https://doi.org/10.1007/s13131-019-1412-8
http://www.hyxb.org.cn
E-mail: hyxbe@263.net

Observed subsurface eddies near the Vietnam coast of the South China Sea

Bo Song[1], Huizan Wang[1, 2*], Changlin Chen[3], Ren Zhang[1], Senliang Bao[1]

[1] College of Meteorology and Oceanography, National University of Defense Technology, Nanjing 211101, China

[2] State Key Laboratory of Satellite Ocean Environment Dynamics, Second Institute of Oceanography, Ministry of Natural Resources, Hangzhou 310012, China

[3] Department of Atmospheric and Oceanic Sciences/Institute of Atmospheric Sciences, Fudan University, Shanghai 200433, China

Received 14 May 2018; accepted 5 July 2018

Abstract

In this study, subsurface eddies near the Vietnam coast of the South China Sea were observed with *in situ* observations, including Argo, CTD, XBT and some processed and quality controlled data. Based on temperature profiles from four Argo floats near the coast of Vietnam, a subsurface warm eddy was identified in spring and summer. The multi-year Argo and Global Temperature and Salinity Profile Programme (GTSPP) data were merged on a seasonal basis based on the data interpolating variational analysis (DIVA) method to reconstruct the three-dimensional temperature structure. There is a warm eddy in the central subsurface at 12.5°N, 111°E below 300 m depth in spring, which does not exist in autumn and is weak in winter and summer. From CSIRO Atlas of Regional Seas (CARS) and Generalized Digital Environment Model (GDEM) reanalysis data, this subsurface warm eddy is also verified in spring.

Key words: coast of Vietnam, subsurface eddy, Argo, GTSPP, DIVA

Citation: Song Bo, Wang Huizan, Chen Changlin, Zhang Ren, Bao Senliang. 2019. Observed subsurface eddies near the Vietnam coast of the South China Sea. Acta Oceanologica Sinica, 38(4): 39–46, doi: 10.1007/s13131-019-1412-8

1 Introduction

Subsurface eddies have a great influence on the distribution of heat, salt, the intensity and position of thermocline, and biogeochemical properties. Subsurface eddies also affect submarine navigation and fishing site selection. The South China Sea (SCS) is the largest semi-enclosed marginal sea in the Northwest Pacific. Many studies have used satellite data to study eddies in the SCS, but the data cannot be used to study their three-dimensional structure. Zhang et al. (2014) pointed out that, excluding the Atlantic, there have been few investigations of subsurface mesoscale eddies in other open oceans or marginal seas. Therefore, it is meaningful to identify subsurface eddies using limited observation data from the SCS.

The surface eddies are frequently observed from remote sensing, however eddies localized in the ocean interior are difficult to detect. Many studies have fully used observational data to discover subsurface eddies. Zhurbas et al. (2004) used CTD data to study the generation of subsurface cyclonic eddies in the Southeast Baltic Sea. Jerónimo and Gómez-Valdés (2007) used *in situ* hydrographic data for July 2004 in the southern region of the California Current and found a subsurface warm eddy. Oka et al. (2009) found a subsurface mesoscale eddy containing anomalously oxygen-rich CMW on the KH-08-3 cruise from October to November 2008. Tang et al. (2012) used a legacy seismic transect in the southern SCS and detected a mesoscale subsurface lens with a center at 450 m depth. Hayes et al. (2014) investigated a subsurface eddy south of Cyprus using ocean gliders. Assassi et al. (2014) used satellite observations only to distinguish subsurface intensified eddies from surface eddies using an index. Research vessels, multiple gliders and mooring-based measurements have been used to study the formation of a subsurface anticyclonic eddy in the Peruvian upwelling regime (Thomsen et al., 2016).

In the SCS, many mesoscale eddies at the surface, such as the Vietnam cold eddy (Yang and Liu, 1998) and Vietnam warm eddy (Fang and Guo, 1998) have been detected. However, studies of subsurface eddies in the SCS are rare due to limited measurement data. Zhang et al. (2014) observed the Southeast Vietnam Offshore Current based on *in situ* CTD and LADCP data during October 2011. In this study, data from Argo and Global Temperature and Salinity Profile Programme (GTSPP) for 2000–2017 were used to study subsurface mesoscale eddies near the coast of Vietnam in the SCS. A subsurface eddy was identified from the Argo temperature profiles. The three-dimensional structure of the eddies can be reconstructed from limited information based on a universal rule (Zhang et al., 2017). In this study, a composite time series (2000–2017) of temperature profiles from Argo and GTSPP was used to reconstruct three-dimensional temperature field based on Data Interpolating Variational Analysis (DIVA), which also identified a subsurface eddy. Reanalysis data from

Foundation item: The National Natural Science Foundation of China under contract Nos 91428206, 41206002, 41706021 and 41775053; the China Postdoctoral Science Foundation under contract No. 2014M551711; the Strategic Priority Research Program of the Chinese Academy of Sciences under contract No. XDA11010103.
*Corresponding author, E-mail: wanghuizan@126.com

CSIRO Atlas of Regional Seas (CARS) and Generalized Digital Environment Model (GDEM) were used to verify the existence of the eddy. The semi-enclosed topography is thought to be an important, but not only mechanism for subsurface eddy genesis in the SCS. There are many possible mechanisms for subsurface eddies. Fang and Guo (1998) points out that the upper circulation of the southern SCS region is mainly driven by the monsoon and topography has a great influence on the subsurface current. Liu et al. (2000) used observational data from a voyage from April to July 1998 and found that in the vicinity at 12°N and 112°E, the upper layer above 300 m formed a cyclone and the lower layer below 500 m formed an anticyclone. Liu et al. (2000) also explained the existence of the coastal jets in summer: eddies are likely to fall off when the jet is unstable. Zhang et al. (2014) hypothesized that the subsurface eddies are generated from upper-layer eddies from horizontal shear of the Southeast Vietnam Offshore Current.

In this study, the subsurface eddies near the Vietnam coast of the SCS were observed by *in situ* observations. There are few previous studies on subsurface eddies in the South China Sea due to little observation data. This study made full use of observation data and detected the subsurface eddy. The paper is organized as follows. In Section 2, data and method are presented. In Section 3, we describe the identification of a subsurface eddy near the coast of Vietnam using Argo buoy observation data. In Section 4, the three-dimensional temperature field is reconstructed in the SCS based on DIVA. In Section 5, reanalysis data from CARS and GDEM are used. This study also discusses the topography effect on subsurface eddies in Section 6.

2 Data and methods

Two sources for ocean observations were used in this study: Argo temperature profiles and GTSPP temperature profiles. Each is described below. Two reanalysis data, CARS and GDEM, are also described.

2.1 *Observation data*

The GTSPP (Sun et al., 2010) temperature profiles are released by the U.S. National Oceanographic Data Center (www.nodc.noaa.gov/GTSPP/). Delayed mode data sources include full resolution data from XBTs, CTDs from the ships, data from Argos, and fully processed and quality controlled data from the organizations that provided real-time low resolution data. We exclude Argo data when we download the delayed mode data from GTSPP, because we used data from the Argo website, which are more complete. GTSPP data removes Argo buoy data and uses the best copy data. The best copy data containing the best temperature and salinity stations are the best quality and highest resolution copies among all data copies. The best copy data files are assembled to provide the most complete data sets without duplication and comprise the best temperature and salinity stations for each month for which data is available in the database. The observation data used in this study covers the period from 2000 to 2017. The Argo temperature profiles were obtained from the Argo Program (www.argo.net).

To study the subsurface eddies near the coast of Vietnam in the SCS, temperature profiles from Argo buoys from January 2000 to October 2017 were used. The study region was 6.56°–24.49°N and 106.39°–121.33°E. According to the Argo buoy trajectories, four Argo buoys were selected based on their drifting tracks passing the coast of Vietnam. The buoy numbers are 2901145 (June 2009–April 2010), 2902697 (November 2016–August 2017), 5904191 (October 2012–December 2013), and 5904747 (May 2016–September 2017), with the time range for each buoy in brackets. The depth stratification of the temperature profile measured in each position was inconsistent. To study the temperature distribution of the cross section, each temperature profile needs to be interpolated to the depth standard layer. The standard layers are 5, 10, 20, 30, 40, 50, 60, 80, 100, 120, 140, 160, 180, 200, 220, 240, 260, 280, 300, 320, 360, 400, 440, 480, 520, 560, 600, 640, 680, 720, 760, 800, 840, 880, 920, 960, 1 000, 1 040, 1 080, 1 120, 1 160, and 1 200 m where an Akima interpolation was used.

2.2 *Reanalysis data*

CARS is an atlas of seasonal ocean water properties. It is derived from a quality-controlled archive of all available historical subsurface ocean property measurements–primarily research vessel instrument profiles and autonomous profiling buoys (www.cmar.csiro.au/cars). With increasing numbers of observation methods in recent years, the CARS mean values are inevitably biased towards the real state of the sea (Ridgway et al., 2002).

In the GDEM-V3.0 (Carnes, 2009), gridded ocean temperature and salinity data were generated by 4.5×10^6 observed T-S profiles dating back to 1920. The denser vertical layers of the GDEM-V3.0 better reflect accurate density profiles than those of coarse resolution models in the deep water, and the data are well suited for studying ocean subsurface eddies (Zhu et al., 2017).

2.3 *The Akima method*

Akima (1970) hypothesized that the interpolated curve obtained from an experienced oceanographer with hand drawing is smooth and natural and is more reasonable than the general interpolated method. Therefore, a manual interpolation method should be used as the standard. Akima further suggested that the results from manual drawings are better because the interpolation primarily considers the size and trends in values of the two measured points adjacent to the interpolation point, instead of all measured points. Accordingly, the author proposed a new interpolation method. The advantage of the Akima method is that only a few data points near the interpolation point are used as control points and the continuity of the derivatives is also considered. The interpolation method is simpler, smoother and more natural than the spline interpolation.

In comparison, linear interpolation only considers the influence of two nearby points. A Runge phenomenon appears in the polynomials interpolation and the cubic spline interpolation method is characterized by a minimum modulus, optimal approximation and convergence, but there will be fluctuation when there is a thermocline in the section. The curve obtained by Akima interpolation method is more natural and smooth than cubic spline interpolation. Therefore, the Akima interpolation method has great advantages for one-dimensional interpolation of the physical ocean.

2.4 *The DIVA method*

DIVA stands for data interpolating variational analysis and is the implementation of variational inverse method (VIM). It is designed to solve 2-D differential or elliptic type variational problems with a finite-element method (Troupin et al., 2012). The field φ minimizes the variational principle over the domain of interest D. Mathematically, gridding consists in determining a field $\varphi(r)$ on a regular grid at position r, using N_d measurements located in r_j, j=1, ..., N_d, i=1, ..., d. The DIVA method contains two parameters,

$$J[\varphi] = \sum_{j=1}^{N_d} \mu_j \left[d_j - \varphi(x_j, y_j)\right]^2 + \|\varphi\|^2 \quad (1)$$

with

$$\|\varphi\| = \int_D \left(\alpha_2 \nabla\nabla\varphi : \nabla\nabla\varphi + \alpha_1 \nabla\varphi \cdot \nabla\varphi + \alpha_0 \varphi^2\right) \mathrm{d}D. \quad (2)$$

The term $\nabla\nabla\varphi : \nabla\nabla\varphi$ of the smoothness constraint has thus the following form in e.g. two dimensions:

$$\begin{aligned} \nabla\nabla\varphi : \nabla\nabla\varphi &= \sum_{i,j=1}^{2} \left(\frac{\partial^2\varphi}{\partial x_i \partial x_j}\right)^2 \\ &= \left(\frac{\partial^2\varphi}{\partial x^2}\right)^2 + 2\left(\frac{\partial^2\varphi}{\partial x \partial y}\right)^2 + \left(\frac{\partial^2\varphi}{\partial y^2}\right)^2, \end{aligned} \quad (3)$$

where α_0 penalizes the field itself (anomalies), α_1 penalizes gradients (no trends), α_2 penalizes variability (regularization), and μ penalizes data-analysis misfits (objective). A weight μ_i can be assigned to each data point d_i. This weight expresses the confidence in a particular data point. It is expressed as a function of the signal-to-noise ratio and correlation length:

$$\mu = \frac{\sigma^2}{\epsilon^2} \frac{4\pi}{L^2}, \quad (4)$$

where σ is signal-to-noise ratio, L is correlation length, and ϵ is errors.

To objectively analyze the subsurface eddy near the coast of Vietnam in the SCS, this study used temperature profile data from Argo buoys and GTSPP from January 2000 to October 2017.

In the previous data introduction, GTSPP data and Argo data were interpolated to 60 standard layers. Before merging two data, quality control is needed first, which includes two aspects. First, the depth in the profiles increases monotonously. Second, profiles with burrs need to be removed; three times standard deviation was used to eliminate profiles with burrs. This method calculates the mean and standard deviation of each standard layer's temperature. Then, a median filter is used for mean and standard deviation. For each standard layer, if the absolute value of the difference between the observed value and mean value is less than three times standard deviation, the profile is left as trusted data, otherwise it will be removed as suspicious. Data from 2000 to 2017 were used and classified by season. Chu et al. (1998) mapped the observational anomaly from a background mean field into a regular grid with a spatial decorrelation scale in the range of 60–90 km. Here, L is 60 km and σ is 0.6. The Argo and GTSPP data were interpolated for season, which contains years of data. Then, DIVA was used to merge the scattered data from the 8-year temperature profiles in each season to obtain the grid data with a resolution of 0.05°.

3 Subsurface eddies based on Argo buoy observation data

In Fig. 1, the blue dotted line represents the trajectory of No. 2901145 buoy and each red spot represents a temperature profile. This buoy drifted from west to east. The time range is from June to July.

For a section composed of red spots, the temperature anomaly is the difference between the observed value and mean value of the standard layer. The section with red dots in Fig. 1 near the coast of Vietnam was used to observe the eddy. The profiles at the red markers were used to draw the temperature anomaly for the section. The eddies along the nearby Vietnam coast are shown in Fig. 2.

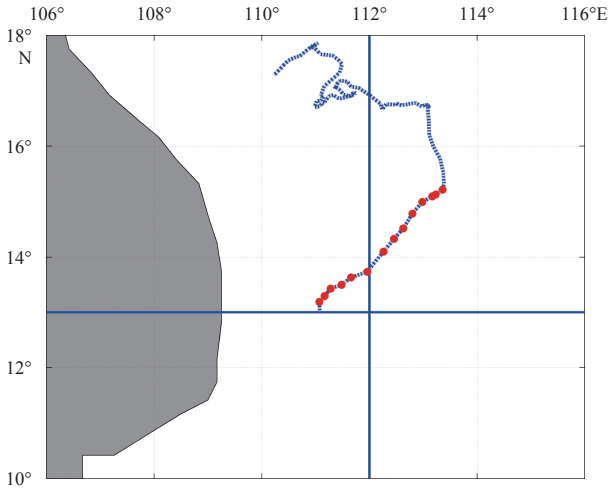

Fig. 1. Drifting trajectory of No. 2901145 buoy. The blue lines are 13°N and 112°E. The points in the position comprise a section. The green line segment is the location where the subsurface eddy can be observed. The result is shown in Fig. 2.

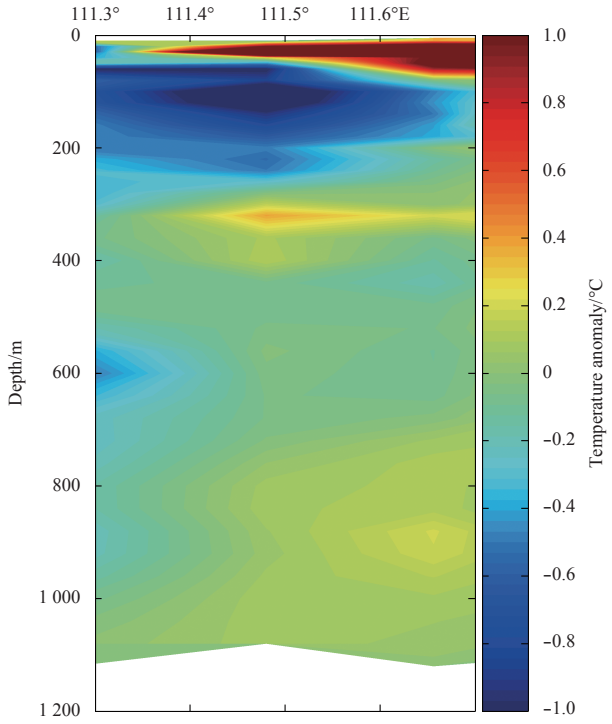

Fig. 2. Temperature anomaly section of No. 2901145 buoy. The cross-section is near the Vietnam coast where a temperature anomaly was identified at the red markers in Fig. 1.

In Fig. 2, a cold eddy is shown above 200 m, and a warm eddy is shown below 300 m. Such a warm eddy is not shown at the surface of the ocean but appears in the subsurface. The same method was applied to the other three buoys, Nos 2902697, 5904191 and 5904747. The drifting trajectory of the buoy (blue dotted line) and selected section position (red point) are shown in Fig. 3.

Figure 4 shows the temperature anomaly distribution of the

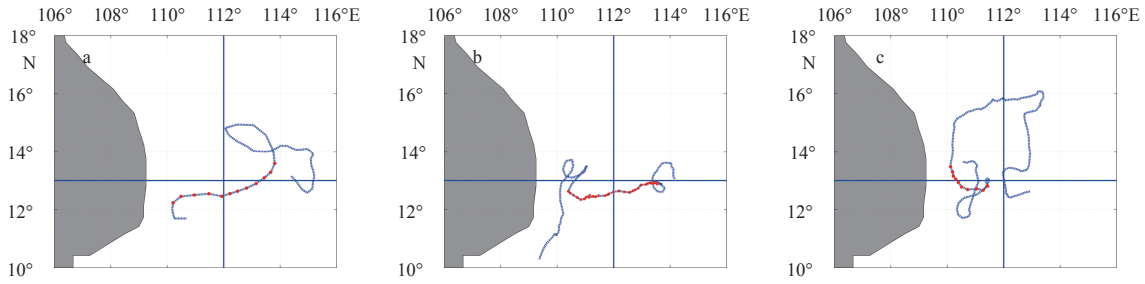

Fig. 3. Drifting trajectory of buoys. a. No. 2902697, b. No. 5904191, and c. No. 5904747. The red markers are the locations of each cross-section. The green line segment is the location where the subsurface eddy can be observed. The results are shown in Fig. 4.

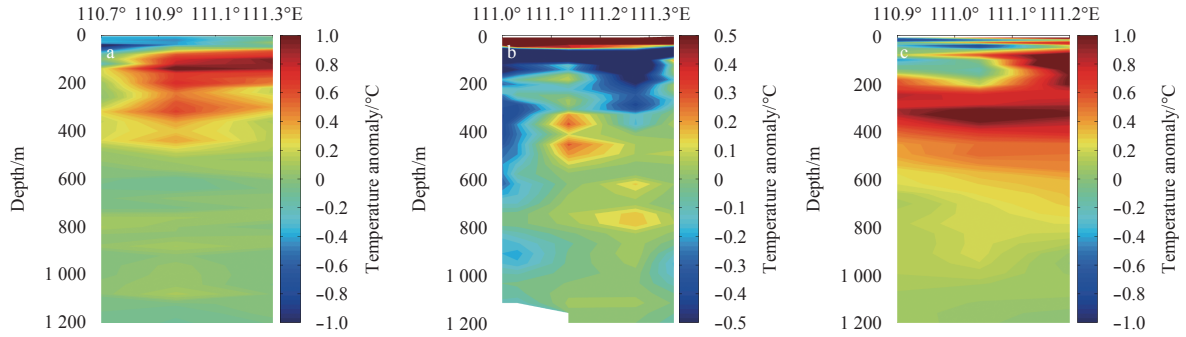

Fig. 4. Temperature anomaly section of three buoys. Intercept the part near Vietnam coast from the temperature anomaly of red spots. a. No. 2902697, b. No. 5904191 and c. No. 5904747.

three buoys. In Fig. 4a, the warm eddy is strong from 100 m to 300 m, but there is no eddy at the surface. In Fig. 4b, the warm eddy stretches from 200 m to 500 m. The warm eddy in Fig. 4b is weaker than the warm eddy in Fig. 4a. In Fig. 4c, the warm eddy stretches from 200 m to 400 m. The time range for the four buoys is spring and summer. The common feature is that there is a warm eddy at the subsurface of the ocean near the Vietnam coast at around 300 m, while it does not exist in the upper layer where there is sometimes a cold eddy.

Satellite observations of sea level anomaly (SLA) from Aviso were used to reveal the surface characteristics corresponding to the described subsurface eddies. Because eddies change slowly over short time periods, the average SLA distributions for different Argo floats are shown (Fig. 5). SLA data update was only available through May 2017, therefore data from Buoy 2902697 from June 1, 2017 to July 30, 2017 was not used. We show the SLA distributions for the remaining three floats here, i.e., 2901145 (June 13–August 4, 2009), 5904191 (March 7–July 9, 2013) and 5904747 (March 30–2017.5.5). As shown in Fig. 5, there is no eddy where the blue lines cross. The satellite data does not show the subsurface eddy detected by the buoys, potentially because the eddy intensities are relatively weak and the subsurface eddy is warm while the eddy at the surface is cold or not present, and subsurface eddies cannot extend to the surface. To further study this subsurface eddy, additional observations were needed.

4 Three-dimensional temperature field reconstruction in the SCS based on DIVA

The interpolation results from March to May are shown in Fig. 6 with depth layers of 50, 100, 200, 300, 400, 480, 600, 680, 800 m. The black dots in the figure indicate where observation data is located. The two blue lines are at 12.7°N and 111.5°E. The intersection of the two lines represents the central position of the eddy. As shown in the diagram, there is a warm eddy at the intersection of blue lines below 300 m. There is no such warm eddy on the surface.

Figure 7 shows the temperature anomaly at 400 m in four seasons. The subsurface warm eddy exists in spring while it does not exist in autumn and is weak in winter and summer at the intersection of the blue lines.

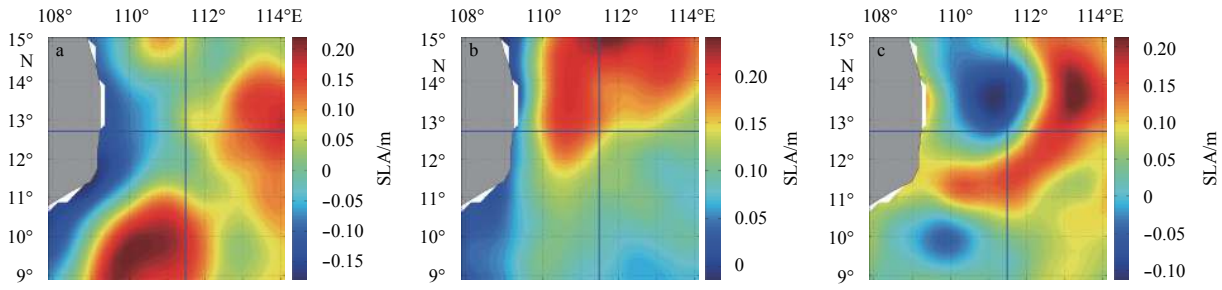

Fig. 5. Sea level anomaly from Aviso. a. No. 2901145, b. No. 5904191 and c. No. 5904747.

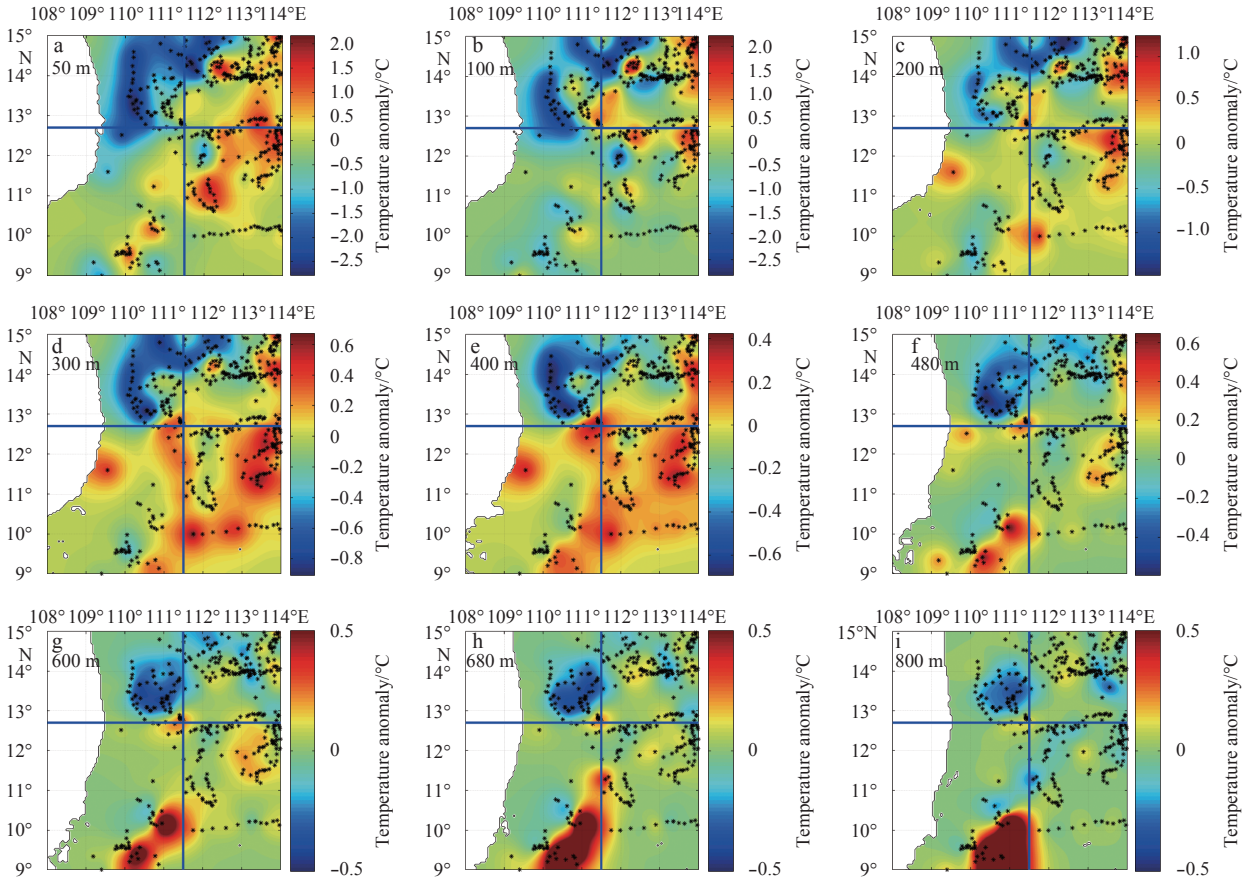

Fig. 6. Temperature anomaly distribution at different depth layers in spring. The depth layers are 50 (a), 100 (b), 200 (c), 300 (d), 400 (e), 480 (f), 600 (g), 680 (h), and 800 m (i).

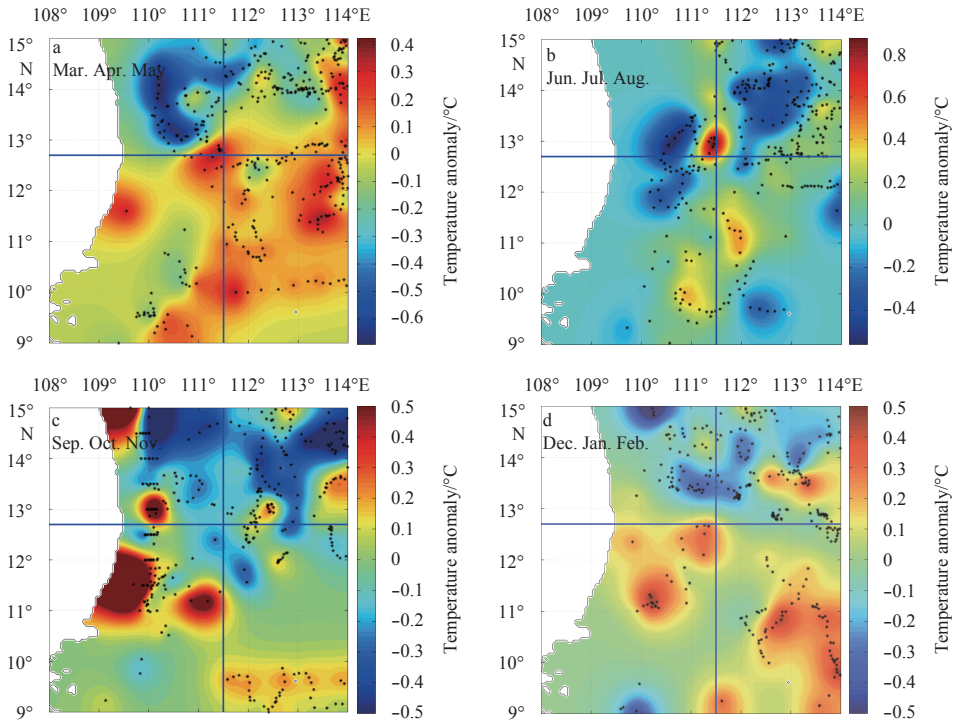

Fig. 7. Temperature anomaly in the 400 m layer in spring (a), summer (b), autumn (c), and winter (d).

5 Reanalysis data from CARS and GDEM

To further to verify the existence of this subsurface warm eddy, CARS and GDEM reanalysis data were used. The 111°E sections of the two reanalysis datasets were selected. Figure 8 shows the 111°E section of the temperature anomaly map. Figures 8a–d show the CARS data in January, April, July, and October, respectively, and Figs 8e–h show the GDEM data for the same months. The Vietnam coast is located around 13°N. The CARS data results show that there is a strong warm eddy in the subsurface near the coast of Vietnam in April at a depth below 300 m, which is not present in the remaining months. The GDEM data also indicates the subsurface warm eddy is the strongest in April near the coast of Vietnam, but also shows the exist in January, although weaker than in April. GDEM data does not show a warm eddy in July and October. The common feature of both the CARS data and the GDEM data is that the subsurface warm eddy is strong in April.

6 Discussion and conclusions

In Fig. 8, the temperature anomalies for the two reanalysis datasets in April, July and October are similar, but the results for January are different, primarily at 100 m. Therefore, the GTSPP-Argo data using DIVA were used to draw the temperature anomaly for the 111°E section in Fig. 9. The GTSPP-Argo results are more similar to the CARS data. The CARS and GDEM reanalysis data have different data sources, quality control methods, and data assimilation methods, so there should be some differences between the results. Nonetheless, the two reanalysis data can elucidate some subsurface eddy characteristics.

There are many reasons for the formation of eddies in the South China Sea. The upper layer circulation over the deep basin of the SCS is driven mainly by the monsoon (Qu, 2000). Wang et al. (2003) classified the geography to gain an overview of eddy generation, with many differences provided, although few could explain the reasons for the generation of subsurface eddies. Topography maybe one of the important reasons but not be the only reason. Wang et al. (2008) suggested that the local wind jets induced by orographic effects could be an important generation mechanism for eddy formation. Xiu et al. (2010) hypothesized that the wind stress curls were an important, but not only, mechanism for eddy genesis in the SCS. The strong negative and positive wind stress curls are caused by the orographic effects. But these eddies mainly refer to the eddies which can be seen from the sea surface. For the subsurface eddies, Oey and Zhang (2004) study the mechanism for the generation of subsurface cyclones when a warm ring smashes onto a continental slope and shelf using a three-dimensional numerical model. Rennie et al. (2007) reveal that at the subsurface about 500 m the undercurrent produced mostly cyclonic eddies due to strong negative vorticity where the current flowed against the continental slope in the model simulations. The topography near the coast of Vietnam is shown in Fig. 10, which has a prominent outward shape. The subsurface topography has a semi-enclosed structure, opening in the east. Subsurface flow is restricted by topography and could be an important reason for eddy formation. Of course, the further study on the mechanism of the subsurface anticyclone eddy needs more high resolution numerical model and more *in situ* observations, and the high resolution realistic modeling should include both open-ocean (e.g., slope current, large eddies, winds and tides) and nearcoast (e.g., river plumes, shelf currents, wind, waves and tides) influences, together with ocean data assimilation (Oey and Zhang, 2004).

This paper used the Argo profile data to generate ocean cross sections near the coast of Vietnam. A warm eddy at the subsurface near the coast of Vietnam was identified via a temperature

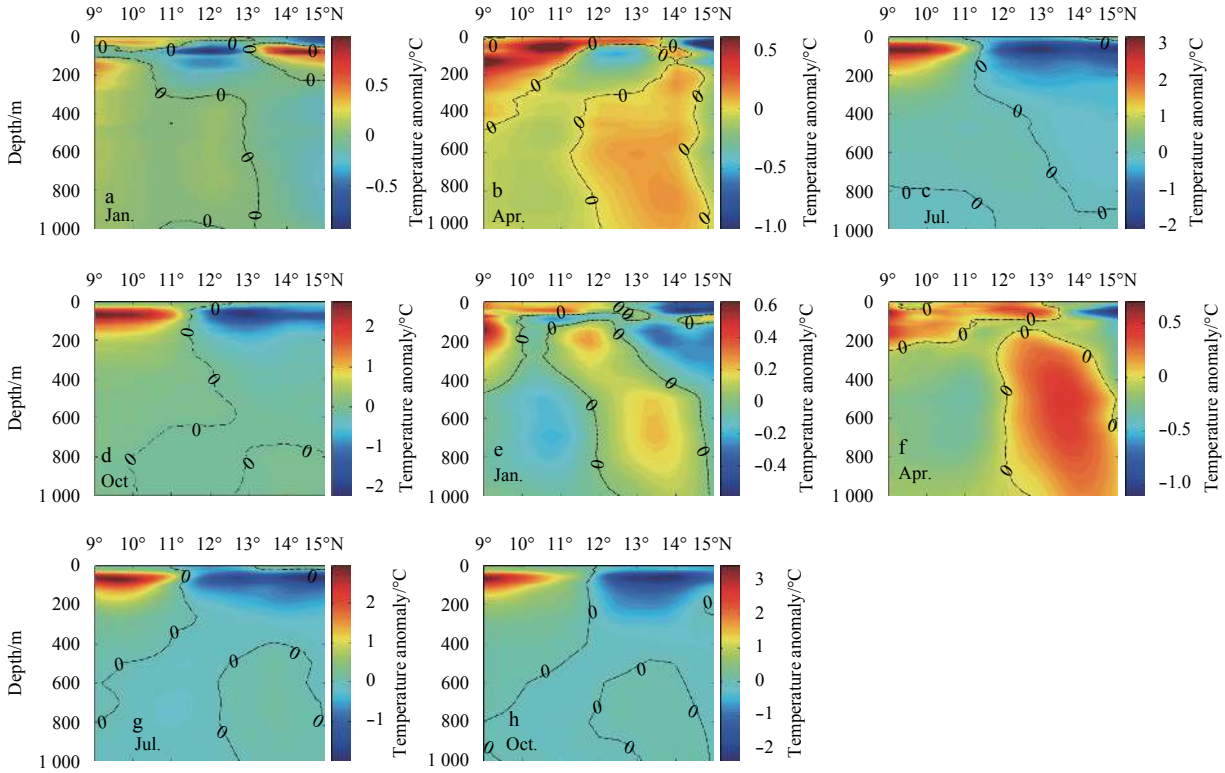

Fig. 8. Temperature anomaly for the 111°E section. a–d. CARS for January, April, July and October, respectively. e–h. GDEM for January, April, July and October, respectively.

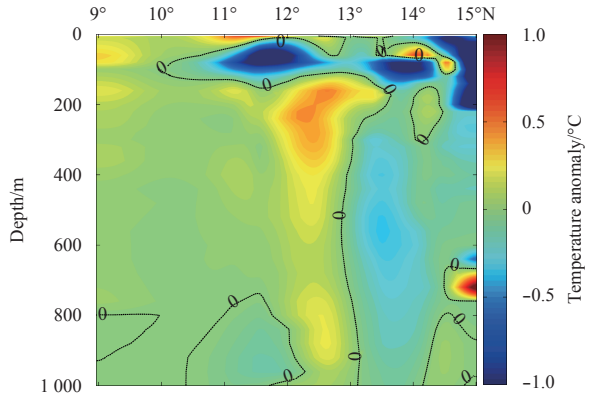

Fig. 9. Temperature anomaly of 111°E section in January using GTSPP-Argo data.

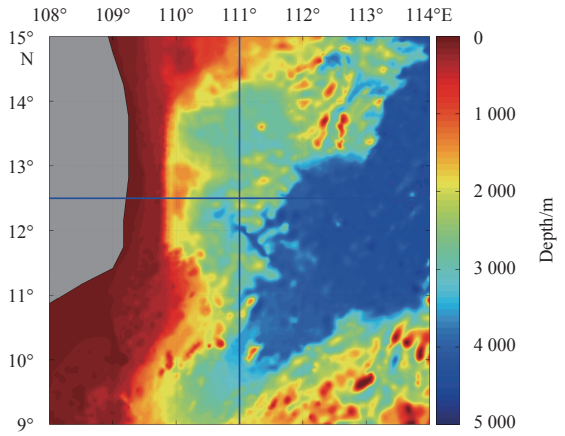

Fig. 10. Coastal topography of Vietnam.

anomaly in the cross section in spring and summer. To study this eddy, several sources of observational data were combined. The 3-D structure of the temperature field in the SCS was reconstructed based on long-term observations from Argo and GTSPP using DIVA. The scatter data were interpolated to standard grid points at standard layer depths. According to the temperature anomalies at different depths, the subsurface warm eddy along the coast of Vietnam can be seen in spring and summer. The center of the warm eddy appears at the subsurface, with no warm eddy at the surface. Based on the CARS and GDEM reanalysis data, a similar phenomenon is also observed. Common features are that the subsurface warm eddy appears along the coast of Vietnam and the warm eddy is strongest in spring. Subsurface eddies are likely to come from other places. Zhang et al. (2014) detected anticyclonic subsurface eddies and hypothesized that it was generated locally by the horizontal shear of the Southeast Vietnam Offshore Current. Zhurbas et al. (2004) conducted numerical experiments and showed that the subsurface cyclone simulated in the Gulf of Gdansk formed due to relaxation of the coastal down welling baroclinic jet. One reason for the formation of a subsurface eddy may be the limitations placed on currents in a semi-closed topography. High resolution numerical modeling and *in situ* observations with high spatial and temporal resolution are needed for further research.

Acknowledgements

We thank Guihua Wang for helpful conversations. We are grateful to several data centers for providing the data used in the study. The Argo float profiles were collected and made freely available by the International Argo Project and the national programs that contribute to it (www.argo.ucsd.edu). Additional information for the profiles was obtained from the Data Management System for the Global Temperature and Salinity Profile Programme (www.nodc.noaa.gov/gtspp/). The CARS Reanalysis data were collected and made freely available by the Commonwealth Scientific and Industrial Research Organization (www.cmar.csiro.au/cars). The GDEM Reanalysis data were made available by the Naval Oceanographic Office.

References

Akima H. 1970. A new method of interpolation and smooth curve fitting based on local procedures. Journal of the ACM, 17(4): 589–602

Assassi C, Morel Y, Chaigneau A, et al. 2014. Detection of subsurface eddies from satellite observations. EGU General Assembly, 2014. Vienna, Austria: EGU

Carnes M R. 2009. Description and Evaluation of GDEM-V 3.0. Memorandum Report. NRL Rep NRL/MR/7330099165, Nav Res Lab, 1–27

Chu P C, Fan Chenwu, Lozano C J, et al. 1998. An airborne expendable bathythermograph survey of the South China Sea, May 1995. Journal of Geophysical Research: Oceans, 103(C10): 21637–21652, doi: 10.1029/98JC02096

Fang Wendong, Guo Zhongxin, Huang Yuting. 1998. Observational study of the circulation observation in the southern of the South China Sea. Chinese Science Bulletin, 43(11): 898–905, doi: 10.1007/BF02884607

Hayes D, Hannides A, Goergiou G, et al. 2014. Description of the long-lived subsurface mesoscale eddy south of Cyprus. In: 6th EGO Meeting and Final Symposium of the Cost Action Es. Kiel, Germany: EGO

Jerónimo G, Gómez-Valdés J. 2007. A subsurface warm-eddy off northern Baja California in July 2004. Geophysical Research Letters, 340(6): L06610

Liu Yonggang, Yuan Yaochu, Su Jilan. 2000. The summer circulation of the South China Sea in the summer of 1998. Chinese Science Bulletin, 45(18): 1648–1655

Oey L Y, Zhang H C. 2004. The generation of subsurface cyclones and jets through eddy–slope interaction. Continental Shelf Research, 24(18): 2109–2131, doi: 10.1016/j.csr.2004.07.007

Oka E, Toyama K, Suga T. 2009. Subduction of North Pacific central mode water associated with subsurface mesoscale eddy. Geophysical Research Letters, 36(8): L08607

Qu Tangdong. 2000. Upper-layer circulation in the South China Sea. Journal of Physical Oceanography, 30(6): 1450–1460, doi: 10.1175/1520-0485(2000)030<1450:ULCITS>2.0.CO;2

Rennie S J, Pattiaratchi C P, Mccauley R D. 2007. Eddy formation through the interaction between the Leeuwin Current, Leeuwin Undercurrent and topography. Deep Sea Research Part II: Topical Studies in Oceanography, 54(8–10): 810–836

Ridgway K R, Dunn J R, Wilkin J L. 2002. Ocean interpolation by four-dimensional least squares-Application to the waters around Australia. Journal of Atmospheric and Oceanic Technology, 19(9): 1357–1375, doi: 10.1175/1520-0426(2002)019<1357:OIBFDW>2.0.CO;2

Sun C, Thresher A, Keeley R, et al. 2010. The data management system for the global temperature and salinity profile programme. In: Hall J, Harrison D E, Stammer D, eds. Proceedings of Ocean Obs'09: Sustained Ocean Observations and Information for Society (Vol. 2). Venice, Italy: ESA Publication WPP-306, doi: 10.5270/OceanObs09.cwp.86

Tang Q S, Wang D X, Li J B, et al. 2012. Image of a subsurface current core in the southern South China Sea. Ocean Science, 9(4): 631–638

Thomsen S, Kanzow T, Krahmann G, et al. 2016. The formation of a subsurface anticyclonic eddy in the Peru-Chile Undercurrent

and its impact on the near-coastal salinity, oxygen, and nutrient distributions. Journal of Geophysical Research: Oceans, 121(1): 476–501, doi: 10.1002/2015JC010878

Troupin C, Barth A, Sirjacobs D, et al. 2012. Generation of analysis and consistent error fields using the Data Interpolating Variational Analysis (DIVA). Ocean Modelling, 52: 90–101

Wang Guihua, Chen Dake, Su Jilan. 2008. Winter eddy genesis in the Eastern South China Sea due to orographic wind jets. Journal of Physical Oceanography, 38(3): 726–732, doi: 10.1175/2007JPO3868.1

Wang Guihua, Su Jilan, Chu P C. 2003. Mesoscale eddies in the South China Sea observed with altimeter data. Geophysical Research Letters, 30(21): 2121, doi: 10.1029/2003GL018532

Xiu Peng, Chai Fei, Shi Lei, et al. 2010. A census of eddy activities in the South China Sea During 1993–2007. Journal of Geophysical Research: Oceans, 115(C3): C03012

Yang H J, Liu Q Y. 1998. The seasonal features of temperature distributions in the upper layer of the South China Sea. Oceanologia et Limnologia Sinica (in Chinese), 29(5): 501–507

Zhang Zhixin, Qiao Fangli, Guo Jingsong. 2014. Subsurface eddies in the southern South China Sea detected from in-situ observation in October 2011. Deep Sea Research Part I: Oceanographic Research Papers, 87: 30–34, doi: 10.1016/j.dsr.2014.02.004

Zhang Zhengguang, Zhang Yu, Wang Wei. 2017. Three-compartment structure of subsurface-intensified mesoscale eddies in the ocean. Journal of Geophysical Research: Oceans, 122(3): 1653–1664, doi: 10.1002/2016JC012376

Zhu Yaohua, Sun Junchuan, Wei Zexun, et al. 2017. A fresh look at the deepwater overflow in the Luzon Strait. Acta Oceanologica Sinica, 36(5): 1–8, doi: 10.1007/s13131-017-1057-4

Zhurbas V, Stipa T, MĠlkki P, et al. 2004. Generation of subsurface cyclonic eddies in the southeast Baltic Sea: Observations and numerical experiments. Journal of Geophysical Research: Oceans, 109(C5): C05033